Structure and short-time dynamics of polydisperse charge-stabilized suspensions

J. K. Phalakornkul, A. P. Gast, and R. Pecora*
Chemical Engineering Department, Stanford University, Stanford, California 94305-5025

G. Nägele, A. Ferrante, B. Mandl-Steininger, and R. Klein
Fakultät für Physik, Universität Konstanz, Postfach 5560, D-78434 Konstanz, Germany

(Received 2 October 1995; revised manuscript received 4 March 1996)

In this work we investigate the equilibrium structure and short-time dynamics of moderately concentrated suspensions of polydisperse charged silica particles immersed in a nearly optically matched solvent. We measure the static structure factor $S_M(q)$ and the first cumulant of the intensity autocorrelation function with static and dynamic light-scattering techniques. From these two quantities we obtain the hydrodynamic function $H_M(q)$ containing the configuration-averaged effects of the hydrodynamic interactions on the short-time dynamics. The experimental results for $H_M(q)$ compare favorably with theoretical calculations based on recent work by Nägele *et al.* [Phys. Rev. E **47**, 2562 (1993); Phys. Rep. (to be published)]. We show that both hydrodynamic interactions and polydispersity significantly affect the short-time dynamics even at small volume fractions. At small wave numbers hydrodynamic interactions slow the initial decay of the intensity autocorrelation function, whereas near the position of the principal peak of $S_M(q)$ the decay rate is enhanced. [S1063-651X(96)09807-8]

PACS number(s): 61.20.Gy, 61.20.Lc, 82.70.Dd, 83.10.Pp

I. INTRODUCTION

Well characterized colloidal suspensions are excellent model systems to understand the influence of interparticle interactions on the structure and dynamics in complex fluids. A considerable amount of theoretical and experimental work on suspensions of hard spheres [1–7] and charged spheres [8–14] provides information about how interactions determine liquidlike and ordered structures and how these structures influence the suspension dynamics. Two types of interactions can be identified: direct interparticle interactions and indirect hydrodynamic interactions (HIs) due to the velocity field generated in the supporting fluid by the particle motions.

A primary technique for studying the static and dynamic properties of these suspensions is light scattering [15]. In monodisperse suspensions the static structure factor $S(q)$ (q is the modulus of the scattering vector) can be determined from measurements of the angular dependence of the mean scattered intensity, provided that the mean interparticle spacing is comparable to the wavelength of light. The peaks in the structure factor indicate spatial correlations among the particles due to the direct forces.

Since Coulombic forces keep highly charged particles far apart, the effects of the short-range hydrodynamic interactions in diluted suspensions of these systems are frequently neglected [9,11,12,16,17]; however, recent theoretical calculations [18,8,19,20] have demonstrated the importance of HIs particularly in charged suspensions. The apparent diffusion coefficient $D(q)$, defined as the ratio of the hydrodynamic function to the static structure factor $H(q)/S(q)$, provides a measure of the short-time dynamics. For negligible HIs, $H(q)$ becomes the Stokes diffusion coefficient D_0 of an isolated sphere and $D(q)$ is due to $S(q)$ only. When HIs are important, $H(q)$ becomes explicitly q dependent. Intuitively, one expects that HIs always lead to a slowing down of the particle density relaxation, e.g., $H(q)/D_0<1$ should hold for all wave numbers. Nonetheless, both experiments [21] and theoretical predictions [18,8,19,20] show that $H(q)/D_0$ can exceed 1 around the principal peak of $S(q)$. The peak value of $H(q)/D_0$ increases with increasing volume fraction ϕ; this behavior differs from that of hard spheres, where the peak value never exceeds one and decreases with increasing ϕ.

All of the studies mentioned above assume that the suspensions were monodisperse. In the process of synthesizing single-component suspensions, a certain degree of size polydispersity is unavoidable and even required in some applications. In general, the size distribution is broader for suspensions of smaller particles. In charged particles, the size polydispersity often gives rise to an associated polydispersity in the surface charge. As a result, both size and charge polydispersity may affect the equilibrium structure and diffusion in the suspensions.

Due to the complexity of polydisperse systems, little is known about their dynamical properties [2,22–25]. A number of experimental investigations have appeared [26–28] on polydisperse charge-stabilized suspensions at low volume fractions, where the influence of HIs has been ignored in the analysis of the experimental data. No reported experimental work on polydisperse systems has encompassed a sufficiently large particle concentration for HIs to be important over an extended range of wave numbers. The primary limitation has been the occurrence of multiple scattering, which invalidates the assumption of single scattering, underlying the conventional interpretation of dynamic light-scattering (DLS) data.

In this work, we investigate the combined effect of HIs

*Present address: Chemistry Department, Stanford University, Stanford, CA 94305-5080.

and polydispersity on the short-time diffusion in polydisperse suspensions of charged silica spheres. In order to eliminate complications from multiple scattering, we nearly matched the refractive index of the spheres with that of a mixed organic solvent. The static and dynamic properties of the suspended silica particles are investigated using static and dynamic light-scattering techniques. We limit our studies to the short-time dynamics where the correlation times are very large compared to the momentum relaxation time, but very small with respect to the structural relaxation of the particles. We apply the method of cumulants to evaluate the dynamic scattering and are able to measure the hydrodynamic function by combining the DLS measurements of the first cumulant with static light-scattering (SLS) measurements of the structure factor. The measured static structure factor is compared with theoretical calculations derived from the hypernetted-chain (HNC) approximation for colloidal mixtures [29]. We model the size polydispersity by a histogram representation of the unimodal continuous Schulz distribution [29,30].

We model the silica particles as hard spheres having an ''effective charge'' Z^{eff} [31] and interacting by a screened Coulomb repulsion of the Derjaguin-Landau-Verwey-Overbeek (DLVO) type [29,32]. The relation between particle size and effective charge is unknown; we explore several models for this dependence and find reasonable agreement when we fit the experimental structure factor with a size-independent Z^{eff}. We model the measurable hydrodynamic function $H_M(q)$ with a pairwise-additivity approximation for the hydrodynamic interaction [18,8].

We show that the short-time diffusion is significantly affected by HIs even at low particle concentrations. The experimental results for $H_M(q)$ confirm the theoretical prediction [18,8] that, when properly normalized, this function is greater than 1 in the neighborhood of the first peak in the static structure factor. We further show that size polydispersity reduces the oscillations of $H_M(q)$ and that this effect is particularly strong for the measurable structure factor at short wave numbers and in the region of the principal peak.

The paper is organized as follows. In Sec. II we briefly describe the polydispersity model and the effective interaction potential used in our calculations. In Sec. III we summarize the SLS and DLS relations for polydisperse suspensions, relevant to our study. There we emphasize the difference between scattering from monodisperse and polydisperse suspensions. In Sec. IV we describe our scheme for calculating $S_M(q)$ and $H_M(q)$. We discuss the sample preparation and experimental methods in Sec. V and present the experimental and theoretical results in Sec. VI. Finally, in Sec. VII we summarize the important findings from our work.

II. MODEL OF POLYDISPERSITY AND INTERACTION POTENTIAL

The size distribution of a one-component suspension of colloidal particles can be conveniently represented by a continuous unimodal Schulz distribution [29,30]

$$p(\sigma;\overline{\sigma},s)=\left(\frac{t+1}{\overline{\sigma}}\right)^{t+1}\frac{\sigma^t}{\Gamma(t+1)}\exp\left(-\frac{t+1}{\overline{\sigma}}\,\sigma\right)\quad (t>0), \tag{1}$$

where $p(\sigma;\overline{\sigma},s)$ denotes the probability distribution for the particle diameter σ and $\Gamma(t)$ is the gamma function. The only two parameters that characterize this distribution are the mean diameter $\overline{\sigma}$ and the relative standard deviation s. The latter is related to the width parameter t by

$$s=\frac{[\langle\sigma^2\rangle-\overline{\sigma}^2]^{1/2}}{\overline{\sigma}}=[t+1]^{-1/2}. \tag{2}$$

The moments of the Schulz distribution are given by

$$\langle\sigma^n\rangle=\int_0^\infty d\sigma\ \sigma^n p(\sigma;\overline{\sigma},s)=\frac{(n+t)!}{t!(t+1)^n}\,\overline{\sigma}^n, \tag{3}$$

with $n=0,1,2,\ldots$. The important features of the Schulz distribution are its skew symmetry towards larger sizes and its approach towards a Gaussian distribution for very small values of s. This skewness allows for good fits of the experimentally determined size distribution in many sorts of colloidal suspensions [18,24,30]. While other choices for the size distribution function exist, the detailed shape of this distribution is not critical for sufficiently small s. The continuous Schulz distribution can be used directly in the calculation of static or dynamic correlations in very diluted systems of practically noninteracting particles [30] or polydisperse hard-sphere mixtures, where one can exploit the analytic expression for the partial structure factors with the Percus-Yevick approximation [33,34]. For charge-stabilized suspensions, we approximate the continuous distribution with a histogram

$$p(\sigma)=\sum_{\alpha=1}^{m} x_\alpha\delta(\sigma-\sigma_\alpha) \tag{4}$$

consisting of a small number m of subcomponents. The mole fraction x_α and the diameter σ_α of each subcomponent are determined by equating the first $2m$ moments of the histogram and the continuous Schulz distribution, i.e.,

$$\sum_{\alpha=1}^{m} x_\alpha(\sigma_\alpha)^l=\langle\sigma^l\rangle,\quad l=0,1,2,\ldots,2m-1. \tag{5}$$

We solve these equations via the equivalent Gauss-Laguerre method. The number m of subcomponents needed depends on the value of s. Three subcomponents are sufficient for the calculation of the static structure factor $S_M(q)$ in a suspension of polydisperse hard spheres [35] and polydisperse charged suspensions [25,29] with $s<0.3$. A minimum of five components is required for the calculation of $H_M(q)$ when s is 0.3. In this work with $s=0.15$, three subcomponents are sufficient to calculate $S_M(q)$ and $H_M(q)$ within the range of our experimentally probed wave numbers, we find no improvement when we increase m up to 12.

The effect of the van der Waals interaction between silica particles suspended in a nearly index-matched solvent is minimal. Thus we neglect the van der Waals forces and describe the effective pair potential, $u_{\alpha\beta}(r)$ between two particles of subcomponents α and β, as a hard sphere plus screened Coulomb potential of the form [8]

$$\frac{u_{\alpha\beta}(r)}{k_BT}=\begin{cases}\infty, & r<\dfrac{(\sigma_\alpha+\sigma_\beta)}{2}\\ L_BZ_\alpha^{\rm eff}Z_\beta^{\rm eff}\left(\dfrac{e^{\kappa\sigma_\alpha/2}}{1+\kappa\sigma_\alpha/2}\right)\left(\dfrac{e^{\kappa\sigma_\beta/2}}{1+\kappa\sigma_\beta/2}\right)\dfrac{e^{-\kappa r}}{r}, & r>\dfrac{(\sigma_\alpha+\sigma_\beta)}{2},\end{cases} \tag{6}$$

where $L_B=e^2/\epsilon k_BT$ is the Bjerrum length, e is the elementary charge, and ϵ is the dielectric constant of the suspending medium. $Z_\alpha^{\rm eff}$ denotes the effective charge (in units of e) of particles in subcomponents α and the equation

$$\kappa^2=4\pi L_Bn\sum_{\alpha=1}^{m}x_\alpha|Z_\alpha^{\rm eff}|+\kappa_{\rm salt}^2 \tag{7}$$

defines the Debye-Hückel screening parameter κ. In writing Eq. (7), we assume that the counterions are monovalent and n is the overall number density of colloidal particles, related to the total volume fraction ϕ according to

$$n=\frac{6\phi}{\pi\langle\sigma^3\rangle}. \tag{8}$$

The screening parameter is determined by dissociating counterions and by the possible presence of added salt. Since we use high-purity organic solvents, we will assume $\kappa_{\rm salt}=0$.

The effective charges entering the DLVO potential are typically smaller than the bare ones [31]. Since we have no *a priori* knowledge of the form of charge polydispersity, we assume that the effective charge of the subcomponent α is related to its size σ_α by

$$Z_\alpha^{\rm eff}=\overline{Z^{\rm eff}}\left(\frac{\sigma_\alpha}{\overline{\sigma}}\right)^\mu, \tag{9}$$

where $\overline{Z^{\rm eff}}$ denotes the mean effective charge. In principle, one could determine the exponent μ by comparison of the experimental and computed $S_M(q)$. In previous work on latex particles [24,25], the value $\mu=2$ was used. Here we test the values $\mu=0,1,2$ and, as explained in detail in Sec. VI, we find $\mu=0$ to be sufficient.

We neglect any possible influence due to electroviscous effects on the short-time diffusion. These effects arise from the distortion of the mobile cloud of counterious around a colloidal particle. The electroviscous effect gives rise to a somewhat increased friction experienced by an isolated colloidal particle only when the double-layer thickness is comparable to the particle radius [36].

III. LIGHT SCATTERING FROM POLYDISPERSE SUSPENSIONS

In this section we briefly summarize those relations of the theory of light scattering relevant to our interpretation of static and dynamic light-scattering data from polydisperse samples. More detailed explanations and derivations can be found in Refs. [8,37]. We start with the relations for SLS and then proceed with those for DLS.

A. Static scattering relations

Extending the scattering relations for a monodisperse system to a polydisperse system of N particles distributed in m different components, we obtain the average scattered intensity

$$I(q)=\left\langle\left|\sum_{\alpha=1}^{m}\sum_{l=1}^{N_\alpha}f_\alpha(q)e^{i\mathbf{q}\cdot\mathbf{R}_l^\alpha}\right|^2\right\rangle, \tag{10}$$

where we have assumed that single-scattering events dominate the signal. In this expression, $\mathbf{R}_l^\alpha$ denotes the position vector of the lth colloidal particle in component α, which consists of N_α particles so that $\Sigma_{\alpha=1}^{m}N_\alpha=N$, and $\langle\,\rangle$ denotes an equilibrium ensemble average. The modulus q of the wave vector $\mathbf{q}$ is related to the scattering angle θ, the solvent refractive index ν_s, and the wavelength λ of the incident light in vacuo by $q=(4\pi\nu_s/\lambda)\sin\theta/2$. For homogeneous spheres in a nearly refractive index-matching solvent, the Rayleigh-Gans-Debye condition

$$\frac{2\pi}{\lambda}\sigma_\alpha\left(\frac{\nu_\alpha}{\nu_s}-1\right)\ll 1 \tag{11}$$

is satisfied and the scattering amplitude of an α-type particle is described by

$$f_\alpha(q)=(\nu_\alpha-\nu_s)\sigma_\alpha^3b(q\sigma_\alpha/2), \tag{12}$$

where ν_α is the refractive index of all the particles with diameter σ_α and the form amplitude $b(q\sigma_\alpha/2)$ of an α-type particle is given by $b(x)=3j_1(x)/x$, where $j_1(x)$ is the spherical Bessel function of first order. In Eqs. (10)–(12) we allow for a size-dependent refractive index ν_α. From Eqs. (10)–(12), the average intensity can be written as [18,8]

$$I(q)=N\overline{f^2}(q=0)\overline{P(q)}S_M(q), \tag{13}$$

where

$$\overline{f^2}(q)=\sum_{\alpha=1}^{m}x_\alpha f_\alpha^2(q) \tag{14}$$

is the second moment of the distribution of the scattering amplitudes and x_α the partial mole fraction. The average form factor $P(q)$ is defined, in analogy with monodisperse suspensions, as

$$\overline{P(q)}=\frac{\overline{f^2}(q)}{\overline{f^2}(q=0)}. \tag{15}$$

The so-called measurable static structure factor $S_M(q)$ in Eq. (13) is a weighted superposition of $m(m+1)/2$ partial structure factors $S_{\alpha\beta}(q)$ according to

$$S_M(q)=\frac{1}{\overline{f^2}(q)}\sum_{\alpha,\beta=1}^{m}(x_\alpha x_\beta)^{1/2}f_\alpha(q)f_\beta(q)S_{\alpha\beta}(q). \tag{16}$$

The partial static structure factors are related to the partial radial distribution functions $g_{\alpha\beta}(r)$ by

$$S_{\alpha\beta}(q)=\delta_{\alpha\beta}+n(x_\alpha x_\beta)^{1/2}\int d^3r\ e^{i\mathbf{q}\cdot\mathbf{r}}[g_{\alpha\beta}(r)-1]. \quad (17)$$

Here $g_{\alpha\beta}(r)$ is the relative probability of finding a β-type particle a distance r from a particle of type α. Slightly different definitions of $S_{\alpha\beta}(q)$ exist in the literature [29,38], but our definition [39,40] ensures that $S_{\alpha\beta}(q\to\infty)=\delta_{\alpha\beta}$ independent of the mole fractions x_α and that $S_M(q\to\infty)=1$. Also with this definition, $S_M(q)$ reduces to $S(q)$ for a monodisperse system. From Eq. (16), it is apparent that the measurable structure factor $S_M(q)$ in polydisperse systems depends on the scattering properties; this dependence contrasts with monodisperse systems where $S(q)$ is a purely statistical mechanical quantity. Indeed, $S_M(q)$ contains information on both the interparticle and intraparticle properties.

We extracted $S_M(q)$ from our SLS measurements by dividing the scattered intensity $I(q;n)$ of the concentrated system by that of the dilute suspension, where $S_{\alpha\beta}(q;n_0)\approx\delta_{\alpha\beta}$ for all q. Hence

$$S_M(q)=\frac{n_0 I(q;n)}{n I(q;n_0)}, \quad (18)$$

where n and n_0 are the number densities in the concentrated and diluted system, respectively. This division procedure is only valid when the size, shape, and scattering properties of the particles are unchanged by dilution. We have assumed that the particles are optically homogeneous and that they all have the same refractive index, regardless of their size. As a consequence of this hypothesis, it follows from Eqs. (14)–(16) that $P(q)$ and $S_M(q)$ should be independent of the refractive index difference $\nu_\mu-\nu_s$ between particles and solvent. This assumption is discussed in Sec. VI.

B. Dynamic scattering relations

The key quantity in the analysis of polarized DLS experiments is the electric field autocorrelation function, given by [37]

$$I(q,t)=N\overline{f^2}(q=0)\overline{P(q)}S_M(q,t) \quad (19)$$

for a polydisperse system. The measurable dynamic structure factor $S_M(q,t)$ is defined, similar to the static case, as [8,37]

$$S_M(q,t)=\frac{1}{\overline{f^2}(q)}\sum_{\alpha,\beta=1}^{m}(x_\alpha x_\beta)^{1/2}f_\alpha(q)f_\beta(q)S_{\alpha\beta}(q,t), \quad (20)$$

ensuring that $S_M(q,0)=S_M(q)$. Here the scattering amplitude $f_\alpha(q)$ is calculated in Eq. (12) and the $m(m+1)/2$ partial dynamic structure factors are

$$S_{\alpha\beta}(q,t)=\frac{1}{(N_\alpha N_\beta)^{1/2}}\langle n^\alpha_{-\mathbf{q}}(0)n^\beta_{\mathbf{q}}(t)\rangle, \quad (21)$$

where

$$n^\alpha_{\mathbf{q}}=\sum_{l=1}^{N_\alpha}e^{i\mathbf{q}\cdot\mathbf{R}^\alpha_l} \quad (22)$$

is the Fourier component of the microscopic density fluctuations of component α. Hence $S_{\alpha\beta}(q,t)$ is a correlation function between α- and β-type particles.

In this work, we are concerned with the dynamics in the short-time limit. Specifically, we consider the time domain in which the hydrodynamic interactions are instantaneous while the appreciable change in the particle configuration due to many-body diffusion does not yet occur. Dynamic light-scattering experiments measure the dynamics of colloidal particles in this time interval, which falls between the momentum relaxation time $[\tau_B=M/(3\pi\eta\overline{\sigma})]$ and the structural relaxation time $[\tau_I=\overline{\sigma^2}/D^0(\overline{\sigma})]$ for an isolated silica sphere of mass M and diameter $\overline{\sigma}$, immersed in a solvent of shear viscosity η, to diffuse with its translational diffusion coefficient $D^0(\overline{\sigma})=k_BT/(3\pi\eta\overline{\sigma})$. In this regime, the fluid exerting friction forces on the particles is incompressible and the equilibrium configuration space-time correlation functions are governed by Smoluchowski equation.

The initial decay of $S_M(q,t)$ is then conveniently analyzed in terms of the cumulant expansion

$$S_M(q,t)=S_M(q)\exp\left[\sum_{l>0}\frac{(-t)^l}{l!}\Gamma^{(l)}_M(q)\right], \quad (23)$$

with the cumulant of order l given by

$$\Gamma^{(l)}_M(q)=(-1)^l\lim_{t\to0}\left[\frac{\partial^l}{\partial t^l}\ln S_M(q,t)\right], \quad (24)$$

where $t\to0$ should be interpreted as $\tau_B\ll t\ll\tau_I$. Consider first a polydisperse suspension of noninteracting homogeneous spheres. Assuming that the sizes are distributed according to the unimodal Schulz distribution, we obtain the following result for the long-wavelength limit of the first and the second cumulant:

$$\lim_{q\to0}\frac{\Gamma^{(1)}_M(q)}{q^2}=\frac{D^0(\overline{\sigma})}{1+5s^2}\approx D^0(\overline{\sigma})[1-5s^2], \quad (25)$$

$$\lim_{q\to0}\frac{\Gamma^{(2)}_M(q)}{[\Gamma^{(1)}_M(q)]^2}=\frac{s^2}{l+4s^2}\approx s^2, \quad (26)$$

where the last approximate equalities are generally valid for small relative standard deviation s. The limit $q\to0$ is practically realized when $q\overline{\sigma}<0.5$. We used Eqs. (25) and (26) to obtain an estimate of the mean particle diameter $\overline{\sigma}$ and the degree of polydispersity s from DLS on a dilute suspension.

At higher concentrations when interactions between particles become important, the first cumulant of $S_M(q,t)$ is used to define a measurable q-dependent diffusion coefficient $D_M(q)$ by

$$D_M(q)=\frac{\Gamma^{(1)}_M(q)}{q^2}. \quad (27)$$

The function $D_M(q)$ is related to the measurable, and scattering-amplitude-dependent, hydrodynamic function $H_M(q)$ as [18,8]

$$D_M(q)=\frac{H_M(q)}{S_M(q)}; \tag{28}$$

this is the polydisperse equivalent of

$$D(q)=\frac{H(q)}{S(q)}, \tag{29}$$

known for monodisperse systems [16]. The measurable hydrodynamic function can be written as [18]

$$H_M(q)=\frac{1}{\overline{f^2}(q)}\sum_{\alpha,\beta=1}^{m}(x_\alpha x_\beta)^{1/2}f_\alpha(q)f_\beta(q)H_{\alpha\beta}(q), \tag{30}$$

where the configuration averaged effect of the HI is contained in the partial hydrodynamic functions $H_{\alpha\beta}(q)$. This follows from the application of the generalized Smoluchowski equation, leading to the expression [18]

$$H_{\alpha\beta}(q)=(N_\alpha N_\beta)^{-1/2}\sum_{l,j=1}^{N_\alpha,N_\beta}\langle\hat{\mathbf{q}}\cdot\mathbf{D}_{lj}^{\alpha\beta}(\mathbf{R}^N)\cdot\hat{\mathbf{q}}e^{i\mathbf{q}\cdot[\mathbf{R}_l^\alpha-\mathbf{R}_j^\beta]}\rangle, \tag{31}$$

where $\hat{\mathbf{q}}=\mathbf{q}/q$. In this expression, the $\mathbf{D}_{lj}^{\alpha\beta}(\mathbf{R}^N)$ are the translational diffusivity tensors, describing the hydrodynamic interactions. In general, the diffusivity tensors depend on the configuration $\mathbf{R}^N$ of all N particles; this renders a full accounting of HIs a difficult task. The quantity $H_{\alpha\beta}(q)$ is known exactly only for vanishingly small hydrodynamic interactions. In this limiting case, $H_{\alpha\beta}(q)=D_\alpha^0\delta_{\alpha\beta}$, where $D_\alpha^0=D^0(\sigma_\alpha)$ is the Stokesian diffusion coefficient of a particle with diameter σ_α. Then, the measurable hydrodynamic function is simply given by an expression

$$H_M^0(q)=\frac{1}{\overline{f^2}(q)}\sum_{\alpha,\beta=1}^{m}x_\alpha f_\alpha^2(q)D_\alpha^0 \tag{32}$$

that depends on quantities that can be determined by light-scattering experiments. Equation (32) is still valid for interacting particles providing that HI are negligible. Furthermore, $H_M^0(q)$ becomes strongly q dependent at larger polydispersity.

It is instructive to separate $H_{\alpha\beta}(q)$ into a self-part and a distinct part [18]

$$H_{\alpha\beta}(q)=\delta_{\alpha,\beta}D_\alpha^s+H_{\alpha\beta}^d(q), \tag{33}$$

where the self-part

$$D_\alpha^s-\langle\hat{\mathbf{q}}\cdot\mathbf{D}_{11}^{\alpha\alpha}(\mathbf{R}^N)\cdot\mathbf{q}\rangle \tag{34}$$

is the short-time tracer-diffusion coefficient of an α-type particle, D_α^s and the distinct part is given by

$$H_{\alpha\beta}^d(q)=(N_\alpha N_\beta)^{1/2}\left(1-\frac{\delta_{\alpha\beta}}{N_\alpha}\right)\langle\hat{\mathbf{q}}\cdot\mathbf{D}_{12}^{\alpha\beta}(\mathbf{R}^N)\cdot\hat{\mathbf{q}}e^{i\mathbf{q}\cdot(\mathbf{R}_1^\alpha-\mathbf{R}_2^\beta)}\rangle, \tag{35}$$

where a representative pair of particles $1\in\alpha$ and $2\in\beta$ has been selected. The distinct part becomes vanishingly small for $q\gg q_m$, where q_m is the position of the principal peak of $S_M(q)$. Hence, according to Eq. (30), $H_M(q)$ is given by a form-amplitude-weighted superposition of tracer-diffusion coefficients in the large-wave-number regime. For strong HIs, $D_\alpha^s<D_\alpha^0$ due to the instantaneous hydrodynamic hindrance associated with the motion of neighboring particles around an α-type particle. The effect of HIs on the short-time tracer-diffusion coefficient is negligible in the case of sufficiently diluted but strongly interacting charge-stabilized suspensions, where $D_\alpha^s\approx D_\alpha^0$ and $H_M(q)/H_M^0(q)\approx 1$ for $q\gg q_m$; however, even for this case strong hydrodynamic interactions persist for intermediate ($q\approx q_m$) and, particularly, for small values of q ($q<q_m$). The ratio $H_M(q)/H_M^0(q)$ is independent of the viscosity η and reduces to $H(q)/D^0$ when all particles are identical. This ratio is thus an indicator of the relative importance of hydrodynamic interactions. When HIs are negligible, this ratio equals 1, as in the monodisperse case, and this implies that the relaxation of density fluctuations is influenced by the direct double-layer forces only. On the other hand, $H_M(q)/H_M^0(q)$ becomes significantly q dependent when the indirect hydrodynamic forces also contribute. We have tested this experimentally by measuring the static structure factor $S_M(q)$ using SLS and the first cumulant [i.e., $D_M(q)$] using DLS.

IV. CALCULATION OF $S_M(Q)$ AND $H_M(Q)$

On the basis of the polydispersity model explained in Sec. II, we calculated the partial radial distribution functions $g_{\alpha\beta}(r)$ and the partial static structure factors $S_{\alpha\beta}(q)$ with the HNC approximation [29,38]. The functions $S_M(q)$ is obtained from $S_{\alpha\mathrm{B}}(q)$ according to Eq. (16). In order to calculate $H_M(q)$, we need to specify the diffusivity tensors $\mathbf{D}_{ij}^{\alpha\beta}(\mathbf{R}^N)$. In principle, these tensors can be obtained by solving the stationary Stokes equation for N hard shperes immersed in an unbound quiescent fluid with appropriate boundary conditions. Unfortunately, this is an extremely difficult task and important advances towards practical numerical results have been achieved only recently [41].

At sufficiently small volume fractions and low amount of excess electrolyte, it is reasonable to assume pairwise additivity of the HI and to approximate the many-body translational diffusivity tensors by [42]

$$\mathbf{D}_{ij}^{\alpha\beta}(\mathbf{R}^N)=\delta_{ij}^{\alpha\beta}\left[D_\alpha^0\mathbf{1}+\sum_{\gamma=1}^{m}{\sum_{l=1}^{N_\gamma}}'\mathbf{A}^{\alpha\gamma}(\mathbf{R}_i^\alpha\cdot\mathbf{R}_l^\beta)\right]+(1-\delta_{ij}^{\alpha\beta})\mathbf{B}^{\alpha\beta}(\mathbf{R}_i^\alpha-\mathbf{R}_j^\beta), \tag{36}$$

where $\delta_{ij}^{\alpha\beta}=0$, whenever the indices $i\in\alpha$ and $j\in\beta$ refer to different spheres, and $\delta_{ii}^{\alpha\alpha}=1$. The prime indicates the exclusion of the terms $\alpha=\gamma$ and $i=l$ from the double sum. Here, we used analytic expressions for the far-field expression of the hydrodynamic tensors $\mathbf{A}^{\alpha\beta}$ and $\mathbf{B}^{\alpha\beta}$ including terms up to r^{-11}. These tensors are expressed as integrals over the partial radial distribution functions $g_{\alpha\beta}(r)$ [18]. The only input needed to calculate $H_{\alpha\beta}(q)$ and hence $H_M(q)$ is $g_{\alpha\beta}(r)$, determined from the HNC approximation. Contrary to suspensions of hard spheres, where $g_{\alpha\beta}(r)$ attains its maximum, at contact, the radial distribution functions $g_{\alpha\beta}(r)$ for charged spheres remain zero for separations comparable to the screening length, due to the electrostatic repulsion.

Therefore, rapid convergence is expected for the series of integrals in the expressions for D^s_α and $H^d_{\alpha\beta}(q)$, whereas for hard-sphere suspensions it is necessary to retain many terms in the inverse distance expansion of $\mathbf{A}^{\alpha\beta}$ and $\mathbf{B}^{\alpha\beta}$. The effect of HIs on D^s_α is expected to be smaller for charged colloidal particles than for uncharged ones due to the r^{-4} leading term in $\mathbf{A}^{\alpha\beta}(r)$: this term remains small for separations where $g_{\alpha\beta}(r)$ is nonzero. On the other hand, $H_M(q)$ at small q is mainly determined by $H^d_{\alpha\beta}(q)$ and is strongly influenced by HIs due to the r^{-1} leading term in $\mathbf{B}^{\alpha\beta}(r)$. Indeed, explicit calculations show that the effect of HIs on $H_M(q)$ is most pronounced for $q \leqslant q_m$ [1]. In the following we will demonstrate that the qualitative behavior of $H_M(q)$ expected from these calculations is consistent with the experiments.

Our calculations of $H_M(q)$ are based on the assumption of pairwise additivity of HIs. In monodisperse systems, the results for $H(q)$ assuming pairwise additivity have been compared with the lowest-order form of the so-called $\delta\gamma$ expansion [43–46]. In this more elaborate method, developed so far only for monodisperse systems, many-body contributions to the HIs are included in an approximate way by a partial resummation of higher-order correlations. The results for $H(q)$ obtained from the $\delta\gamma$ expansion agree well with those obtained assuming pairwise additivity for volume fractions below 0.05 [18,8,19,20]. Hence, we assume that pairwise additivity is also a good approximation for the corresponding polydisperse charge-stabilized suspensions at moderate volume fractions.

V. EXPERIMENT

A. Particle characterization and sample preparation

1. Particle characterization

We used silica spheres coated with 3-trimethoxy-silyl-propyl-methacrylate (TPM) as our model charged spheres. The same batch of spheres was studied previously and the detailed synthesis was reported elsewhere [47]. The seed silica spheres were produced according to the method of Stöber, Fink, and Bohn [48] and followed by the seeded growth procedure of Bogush, Tracy, and Zukoski [49]. Finally, the particles were coated according to the procedure of Philipse and Vrij [50]. The spheres were originally suspended in ethanol and the ethanol was later replaced with dimethylformamide (DMF) (Aldrich, HPLC Grade).

Previous experiments [51] have shown that the silica particles suspended in alcohol carry a surface charge. The charges originate from the surface silanol groups, which are relatively acidic in the presence of ammonia, a reactant in the synthesis. Once the particles are coated with organic chains, such as poly(12-hydroxystearic acid) or (TPM), and suspended in a less polar solvent, the charge density drops dramatically [6,21]. In some cases, the coated silica particles left with a negligible surface charge provide a model for hard spheres [6]. In other cases, a small charge remains on the surface because of the incomplete reaction of the silanols. For example, the estimated ζ potential of the TPM-coated spheres suspended in ethanol is 200 mV, while the potential in 70% by volume of toluene-ethanol solvent is 60 mV [21]. We could not measure the ζ potential of our spheres in the mixed solvent of DMF-pyridine with electrophoresis because the particles were invisible at dilute concentrations; however, the measurements of $S_M(q)$ and the observation of ordering at a volume fraction of 0.12 convince us that our TPM-coated spheres are charged in the mixed solvent. We estimated the effective surface charge from comparison of the acquired $S_M(q)$ with the theoretical calculations.

The seed silica spheres synthesized from Stöber, Fink, and Bohn's recipe are known to be optically isotropic but slightly optically inhomogeneous. For the silica spheres coated with TPM, the inhomogeneity is greater than for the bare particles due to the difference in the refractive indices of the silica core and the TPM layer. In fact, Philipse, Smits, and Vrij [52] found that, for a silica sphere of 83 nm core radius with 6-nm TPM coating thickness, the refractive index difference was on the order of $6\times10^{-3}\pm2\times10^{-3}$.

We followed the work of Tracy and Pecora [47] to match the refractive index of the spheres with their environment and measure the index of refraction of the spheres. They were able to minimize turbidity from highly scattering spheres suspended in DMF at high concentrations by adding pyridine. To determine the index-matching condition, we checked for the absence of multiple-scattering events within the sample. For this purpose, we measured the depolarized component of the scattered light with a Fabry-Pérot interferometer. Since the light source was polarized, any depolarized component was an indication of multiple scattering. We used the apparatus described in Refs. [53,54] to detect the depolarized components of the light scattered from the suspensions at 488-nm wavelength. If the spectra indicated depolarized scattering, we adjusted the solvent refractive index by adding DMF or pyridine. The matching refractive index was calculated from the final solvent composition.

2. Sample preparation

We prepared a dust-free suspension in a 2.54-cm-diam, cylindrical, quartz light-scattering cuvette cell as follows. The cuvette cells were first placed in a solution of 30% hydrogen peroxide and 70% sulfuric acid overnight. We then used a peristaltic pump (375A SAGE instrument) to filter deionized, distilled water into the cell continuously for 2 days. A Millipore disposable polytetrafluoroethylene (PTFE) filter with 0.01 μm-pore size was used. After that we cleaned the cells with 20 ml of filtered absolute ethanol and 20 ml of filtered DMF consecutively. To ensure that the cell was dust free, we placed it in the laser beam and checked for scattering from dust by observation of the scattering volume with a $5\times$ lens.

We prepared a dilute suspension of volume fraction $\phi=10^{-4}$ for particle characterization by diluting a concentrated sphere suspension in DMF with filtered solvent. We used a 0.45-μm PTFE filter to add the sample to the dust-free cell. Before the sample was added, we cleaned the filter by passing 10 ml of DMF through it. We collected about 1 ml of the dilute suspension and kept the sample in a desiccator overnight. The concentrated samples for the dynamic studies were prepared by concentrating a stock solution with $\phi=0.02$ in DMF-pyridine. In order to make a dust free suspension of greater particle concentration, we filtered about 4 ml of the stock solution in to a dust-free cylindrical light-scattering cell prepared as described above. We then centrifuged the cell at 1000 rpm for 30 min at room temperature

with an SS-3 SORVALL centrifuge. When most of the particles settled for form a gel-like sediment at the bottom of the cell, we withdrew the clear supernatant. Then the cuvette cell was shaken by a shaker (Burrell model 75) until the particles were completely resuspended. After that, we added another 4 ml of the filtered stock solution and repeated the contrifuging and resuspending process. When we had collected about 1 ml of the dense suspension, we withdrew the supernatant and measured the suspension weight and calculated the volume fraction of the sample by considering the sediment volume fraction to reflect random close packing, $\phi=0.64$ [55], and taking 0.9546 g/ml as the matching solvent density and 1.6 g/ml as the particle density [50]. The suspension was stepwise diluted for static and dynamic light-scattering experiments. We performed the dilution with slightly different solvent compositions as described below in order to eliminate multiple scattering completely.

B. Methods

Three techniques allowed us to independently determine the particle size and the particle size distribution from a dilute suspension: transmission electron microscopy (TEM), dynamic light scattering, and static light scattering. We used a suspension in ethanol for the microscopy study and a dilute suspension in DMF and matching pyridine-DMF for light-scattering studies. The light scattered from concentrated suspensions contains information on both static and dynamic properties of the system. The static information can be extracted from the intensity and angular distribution of the scattered light, while the dynamic information is contained in its spectral analysis. Therefore, we employed SLS to obtain $S_M(q)$ and performed DLS to acquire $D_M(q)$ of the suspensions in the index-matching solvent. We used depolarized light scattering with interferometry to confirm that single scattering was dominant in our samples.

1. Transmission electron micrographs

Transmission electron micrographs were obtained from particles retained on copper 400 mesh electron microscope grids. We put two drops of a dilute suspension on each grid. After the ethanol had evaporated, the particles left on the carbon-coated Formvar films were photographed. Fifteen different areas from three grids were photographed with an electron microscope Philips EM 400 operating at 100 KV at a magnification of 17 000 calibrated with a diffraction grating. Then we magnified the recorded pictures so that the particle radii could be measured within ± 0.001 μm. Assuming that the particles had a spherical shape, we measured diameters of 486 particles to determine a number-averaged particle radius and a histogram of the size distribution.

2. Light scattering

Both dynamic and static light-scattering experiments used a Lexel argon laser (Model 95) operating at 250 mW at either of the two lines: 457.9 and 514.5 nm. The vertically polarized incident light passed through the index-matching fluid ($\nu=1.452$) in which the sample cell was immersed. The temperature was controlled at 25.0 °C$\pm$0.1 °C. We detected the scattered light with a photomultiplier tube (PMT) mounted on a Brookhaven Instruments BI200 photogoniometer.

In *static light-scattering* experiments, we collected mean intensities as functions of the scattering angles in the range $40° \leqslant \theta \leqslant 130°$. We used the largest pinhole (3000 μm) before the PMT to increase the scattering volume, thereby reducing the effects of reflections from the glass wall. Since the alignment of the goniometer is the critical factor in the angular dependence of the intensity [56], we tested the alignment of our apparatus with an aqueous suspension of well-characterized colloidal polystyrene particles [57], and verified this form factor with Mie scattering theory.

According to the discussion in Sec. III A, the static structure factor $S_M(q)$ is the ratio of the mean intensities collected from a concentrated sample to that measured after dilution, where interactions between colloidal particles can be neglected. The scattering from our indexed-matched suspension was insufficient to measure $P(q)$ in the absence of interparticle interactions. We therefore calculate $P(q)$ assuming Rayleigh-Gans-Debye scattering from spheres having a Schulz distribution of diameters.

In *dynamic light-scattering* experiments, we measured the intensity autocorrelation function as a function of scattering vector. The analysis of the fluctuations was carried out with a Brookhaven BI9000AT digital correlator. Unlike the SLS setup, DLS requires the area of the detector placed in the far field to be equal to one coherent area [15]. We fulfilled this criterion by using the smallest pinhole size 50 μm. The measurable diffusion coefficient $D_M(q)$ was obtained from the first cumulant $\Gamma_M^{(1)}(q)$ as discussed in Sec. III B. A study of a dilute suspension in DMF and in the index-matched pyridine-DMF provided the values of the average free-particle translational diffusion coefficients $D^0(\overline{\sigma})$ according to Eqs. (25) and (26). We then calculated the average hydrodynamic radius (R_h) according to the Stokes-Einstein relation. We took the normalized second cumulant $\Gamma_M^{(2)}(0)/[\Gamma_M^{(1)}(0)]^2$ as another measure of the degree of polydispersity s.

C. Order-disorder transition

While preparing a concentrated suspension in a index-matching DMF-pyridine mixture, we also observed ordering in the transparent sample. At a volume fraction larger than $\phi=0.2$, the suspension was very viscous and gel-like and bubbles were trapped inside for more than 2 days. The time-averaged correlation functions measured from this sample were nonergodic and never decayed to the base line. When the sample was diluted to $\phi=0.1$–0.2, the correlation functions decayed to the base line but varied with the location of the scattering volume under investigation. This is another feature of nonergodic medium, in which the scatterers are localized in a restricted region of phase space [58].

Within these suspensions, the incident light was reflected from some bright speckles, presumably faces of crystallite or crystalline defects. The speckles reappeared under the laser beam a few hours after being shaken. With room light, the transparent liquid looked blue at certain viewing angles. This observation is similar to that of an ordered suspension of monodisperse TPM-coated SiO_2 in an ethanol-toluene mixture [50]. Although our suspensions are polydisperse, we be-

TABLE I. Mean particle radii and size distribution widths as measured by three techniques.

Technique	Solvent	Average radius (nm)	Relative standard deviation s
TEM	dried from ethanol	54.0	0.17[a]
DLS	DMF	60.0	0.12[b]
DLS	31.8% pyridine-DMF	62.0	0.15[b]

[a]From the fit of the experimental histogram with a unimodal continuous Schulz distribution.
[b]From the normalized second cumulant.

lieve a crystal-like structure is formed due to the long-range electrostatic repulsion. Previous researchers have reported the crystallization of polydisperse suspensions of highly charged polystyrene particles [59].

VI. RESULTS AND DISCUSSION

A. Particle size distribution and form factor

Table I summarizes our results for the average radius $\overline{\sigma}/2$ and the relative standard deviation s (''polydispersity''), derived according to three different methods: TEM and DLS. The mean radius determined by TEM is smaller than that obtained from DLS, as already noted in previous work on various types of coated silica particles [51,60,61]. The smaller radius obtained from TEM is probably due to the shrinkage of particles after desolvation and radiation damage. On the other hand, the hydrodynamic particle radius determined from DLS is expected to be somewhat larger than the actual particle radius because of stationary solvent molecules at the surface.

The relative standard deviation s is a measure of the intrinsic width of the size distribution. In our TEM measurement, s was determined by fitting the two-parameter continuous Schulz distribution to the experimentally determined histogram of particle sizes. The best fit yields $s=0.17$, as shown in Fig. 1.

We also determined s from a cumulant analysis of our DLS measurements. From this method we obtain $s=0.12$ and 0.15, respectively (see Table I). The fact that the size

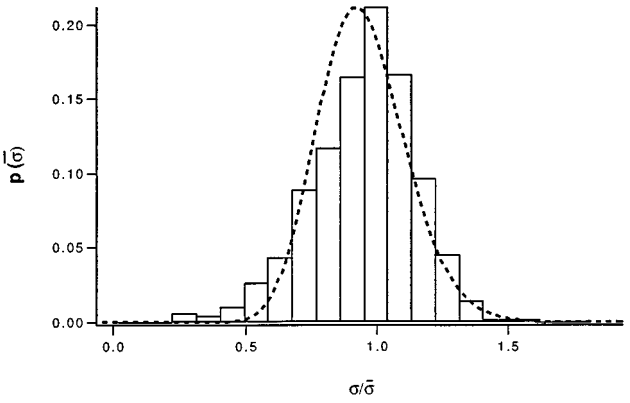

FIG. 1. Comparison of the measured particle size distribution $p(\sigma)$ obtained from TEM (histogram), with the continuous Schulz distribution (dashed line) evaluated for $\overline{\sigma}=108$ nm and $s=0.17$ (cf. Table I).

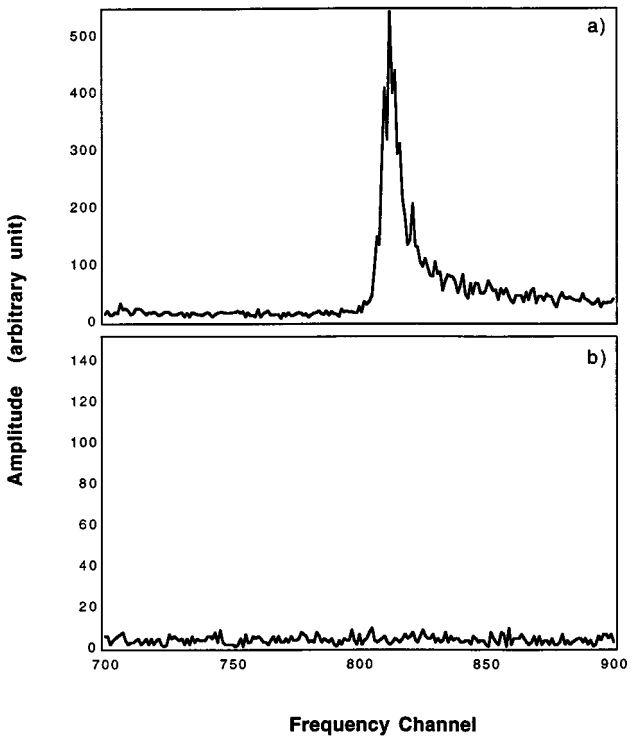

FIG. 2. Spectrum of depolarized scattered light from Fabry-Pérot interferometry: (a) suspension with volume fraction $\phi=10^{-3}$ in pure DMF and (b) suspension with $\phi=7.1\times10^{-2}$ at nearly index-matching conditions in a 29.7% pyridine-DMF mixture.

distributions obtained from both experimental techniques are consistent indicates that there are no large aggregates. The degree of polydispersity is consistent with the work of Philipse and Vrij [50], who reported an increasing degree of polydispersity for smaller silica particles. These researchers found, indeed, a value of polydispersity $s=0.16$ for bare silica particles of average radius 60 nm, synthesized with the Stöber-Fink-Bohn method.

B. Single-scattering indication and index matching

Figure 2 shows two spectra from the Fabry-Pérot interferometry experiments. In Fig. 2(a) we show the spectrum gathered from a cloudy suspension of volume fraction $\phi=10^{-3}$ in pure DMF (see Table III). On the same scale as Fig. 2(a), Fig. 2(b) illustrates the spectrum obtained at the same wavelength from silica particles with $\phi=0.071$ suspended in a 29.7% pyridine-DMF mixture. After performing SLS and DLS experiments on this sample, we diluted the suspension to a volume fraction of $\phi=0.057$ by adding a solution of 31% pyridine-DMF. In order to minimize the depolarized component of the scattered light, the pyridine concentration was enhanced. The sample at concentrations $\phi=0.071$ and 0.057 were index matched at both 488- and 514.5-nm wavelengths while the sample at $\phi=0.039$ was index matched at 488- and 457.9-nm wavelengths. The matching solvent compositions did not vary with different wavelengths.

Measuring the refractive index of the matching solvents using an Abbe refractometer (Bausch and Lomb), we were unable to detect any difference in refractive index among them. For this reason we have estimated the refractive index

TABLE II. Histogram representation of the continuous Schulz distribution for $s=0.15$ and $\overline{\sigma}=124$ nm. The number of components in the histogram is 3. The diameters and the mole fractions of each subcomponent are displayed.

Subcomponent diameters σ_α (Å)	Relative diameters $\sigma_\alpha/\overline{\sigma}$	Mole fractions x_α
$\sigma_1=976.2$	0.787	0.249
$\sigma_2=1277.1$	1.030	0.646
$\sigma_3=1634.1$	1.318	0.105

of each sample (Table III), as a function of solvent composition, employing the empirical Gladstone-Dale equation [62]

$$\left(\frac{1}{n_{\rm mix}}\right)(\nu_{\rm mix}-1)=\left(\frac{W_{\rm DMP}}{n_{\rm DMP}}\right)(\nu_{\rm DMP}-1)+\left(\frac{W_{py}}{n_{py}}\right)(\nu_{py}-1), \tag{37}$$

where W_i is the weight fraction of component i in the mixture.

C. Static structure factor

The parameters entering the polydispersity model, namely, the average particle size and the standard deviation of the particle size distribution are summarized in Table I. In our HNC calculation, we took 62 nm as the average particle radius and $s=0.15$ as the standard deviation. The mole fractions and the sizes of the three subcomponents employed in the discretized Schulz distribution are shown in Table II.

Among the other parameters entering the effective potential, the Bjerrum length L_B can be determined from the bath temperature (25 °C) and the dielectric constant of the solvent mixture, evaluated as a weighted average of the dielectric constants of the pure components (see Table III). The values reported for the Bjerrum length varied slightly with the sample concentration, but this is not critical and we could adopt an average value without any significant difference in the results. Since we have no *a priori* knowledge of the effective charge $\overline{Z}^{\rm eff}$ and the experimental uncertainty in volume fraction ϕ is much larger than the error in the average size or polydispersity, we simultaneously adjust $\overline{Z}^{\rm eff}$ and ϕ to fit the data with our HNC approximation $S_M(q)$. The height of the principal peak is mainly affected by the former, while the peak position is controlled by the latter. The computation was repeated for each of the three proposed size dependences for the effective charge polydispersity ($\mu=0,1,2$).

In Fig. 3, we show the structure factors $S_M(q)$ from the measured $I(q)$ divided by our calculated $P(q)$. They agree well with the HNC structure factors with $\mu=0$. We report the parameters from our fits in Table III. The adjusted values $\phi_{\rm fit}$ for the volume fraction compare well with the experimentally estimated values $\phi_{\rm expt}$. The mean effective valency $\overline{Z}^{\rm eff}$ suggests that the particles carry a large surface charge.

It should be noted that our use of the HNC approximation, although legitimate for this fitting procedure, might lead to an overestimate of about 20% for the value of $\overline{Z}^{\rm eff}$, in comparison with what one would obtain by fitting the same data with a Monte Carlo simulation or a more accurate approximation [63]. Hence we estimate that the actual effective valencies of our system are lower than those obtained from our fits. In any case, our particles are strongly charged and this greatly influences the structure of the suspension.

We made no attempt to improve on the particle surface charges since we only aim to get a reasonable fit to obtain the partial radial distribution functions and partial structure factors necessary to determine the dynamic properties. Although we have supposed in our calculations that $\kappa_{\rm salt}=0$, a small amount of residual salt still provides a consistent fit, with a slightly larger mean effective charge.

In Fig. 3 we also include a comparison of the size polydisperse model ($s=0.15$) with a corresponding monodisperse system of the same average diameter and the same effective charge at each concentration. The effect of the intrinsic size polydispersity is to broaden the principal peak in the structure factor $S_M(q)$, to reduce its height, to slightly shift its location to smaller wave numbers, and to strongly increase the value observed at small q. These trends can be understood by examining how the partial structure factors $S_{\alpha\beta}(q)$ of each subcomponent contribute to the average $S_M(q)$, following a similar analysis given by D'Aguanno and Klein [29].

For this purpose, we also show our HNC results for the $S_{\alpha\beta}(q)$ of sample (c) in Fig. 4. Note that $S_M(q)$ is a

TABLE III. Comparison of the particle volume fractions obtained from sample preparation $\phi_{\rm expt}$ and $S_M(q)$ calculations $\phi_{\rm fit}$. The solvent compositions in each sample, their dielectric constants, and their refractive indices are displayed. The mean effective charge $\overline{Z}^{\rm eff}$ and the Bjerrum length L_B used in the calculations are reported.

Sample	Volume fraction $\phi_{\rm expt}$	Volume fraction $\phi_{\rm fit}$[c]	Solvent composition	Solvent ϵ[a]	L_B (Å)	Solvent ν[b]	$\overline{Z}^{\rm eff}$ (HNC)	λ (nm)
(a)	0.039	0.033	31.7% pyridine-DMF	28.97	19.34	1.453	220	457.9
(b)	0.057	0.048	30.3% pyridine-DMF	29.31	19.32	1.452	220	514.5
(c)	0.071	0.063	29.7% pyridine-DMF	29.46	19.28	1.451	220	514.5
(d)	10^{-4}		31.8% pyridine-DMF	28.94	19.35	1.453		457.9
			100% pyridine	12.30	45.53	1.508		
			100% DMF	36.71	15.25	1.428		

[a]From the Gladstone-Dale equation.

[b]Density-weighted values.

[c]From the best fit of the experimental $S_M(q)$, using the HNC approximation.

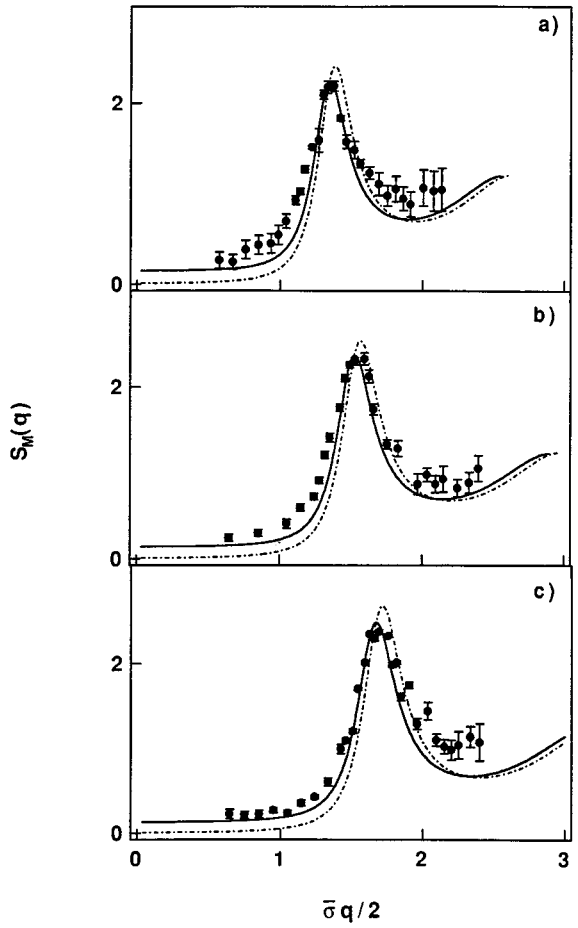

FIG. 3. Comparison of the measurable static structure factor $S_M(q)$ obtained from $I(q)$ divided by $P(q)$ for the Shulz distribution of spherical particles with the calculated one from the HNC approximation. Filled circles, SLS results; full line, INC approximation, assuming $s=0.15$ size polydispersity; dash-dotted line, HNC approximation with $s=0$. The polydispersity model introduced in Sec. II was used, with $\bar{\sigma}=124$ nm, $m=3$, $\kappa_{\text{salt}}=0$, and $\mu=0$ (no charge polydispersity). The three panels correspond to samples at different volume fractions: (a) $\phi_{\text{expt}}=0.039$, (b) $\phi_{\text{expt}}=0.057$, and (c) $\phi_{\text{expt}}=0.071$. See Table III for the values of the wavelength λ used in the experiment and the values of the parameters giving the best fit, i.e., volume fraction ϕ_{fit} and effective charge Z^{eff}, from the HNC calculations.

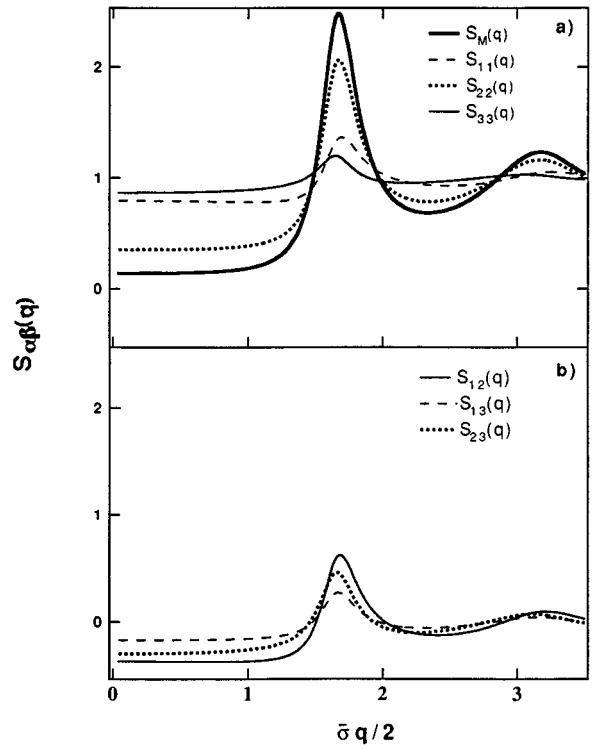

FIG. 4. HNC partial static structure factors $S_{\alpha\beta}(q)$ for sample (c) in Table III; $\phi_{\text{fit}}=0.063$, $Z^{\text{eff}}=220$, $\bar{\sigma}=124$ nm, $s=0.15$, and $\mu=0$. The corresponding partial diameter and mole fraction of each subcomponent are reported in Table II. Top panel: average structure factor $S_M(q)$ and like components $\alpha=\beta$. Bottom panel: unlike components $\alpha\neq\beta$.

weighted sum of partial structure factors, where each subcomponent is weighted by a factor of $x_\alpha^{1/2} f_\alpha(q)$, which scales, in the case of optically homogeneous spheres, like the diameter σ_α to the third power. According to Fig. 4 and Table II, the largest contribution to $S_M(q)$ at low q arises from the largest particles. Moreover, one can see that the six $S_{\alpha\beta}(q)$ are to some extent out of phase causing the lowering and broadening of the principal peak of $S_M(q)$.

From the physical point of view, it is more instructive to consider the corresponding partial radial distribution functions $g_{\alpha\beta}(r)$, related to $S_{\alpha\beta}(q)$ by Eq. (17). For illustration, the three $g_{\alpha\alpha}(r)$ for the like subcomponents are displayed in Fig. 5. Note that the large particles exhibit stronger spatial correlations, i.e., a somewhat larger peak height shifted to a larger distance. This is due to a similar ordering in the strength of the particle potential $u_{11}(r)<u_{22}(r)<u_{33}(r)$ defined in Eq. (6), arising from the geometrical factors $e^{\kappa\sigma_\alpha/2}/(1+\kappa\sigma_\alpha/2)$. In contrast to $g_{\alpha\beta}(r)$, the corresponding ordering of $S_{\alpha\beta}(q)$ is also explicitly affected by the partial mole fractions, through the factors $(x_\alpha x_\beta)^{1/2}$ as written in Eq. (17).

As an illustration of the influence of charge polydispersity on the structure, Fig. 6(a) displays the influence on the width of $S_M(q)$ from varying μ only, keeping all the other parameters fixed as in Table III. Only the peak height and the small

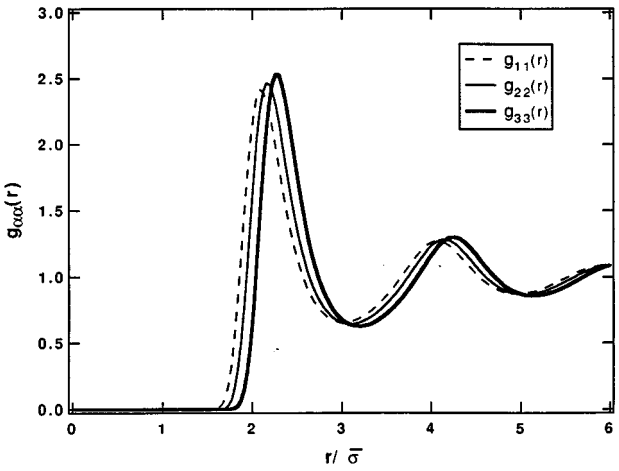

FIG. 5. Partial radial distribution functions $g_{\alpha\alpha}(r)$ for sample (c) in Table III.

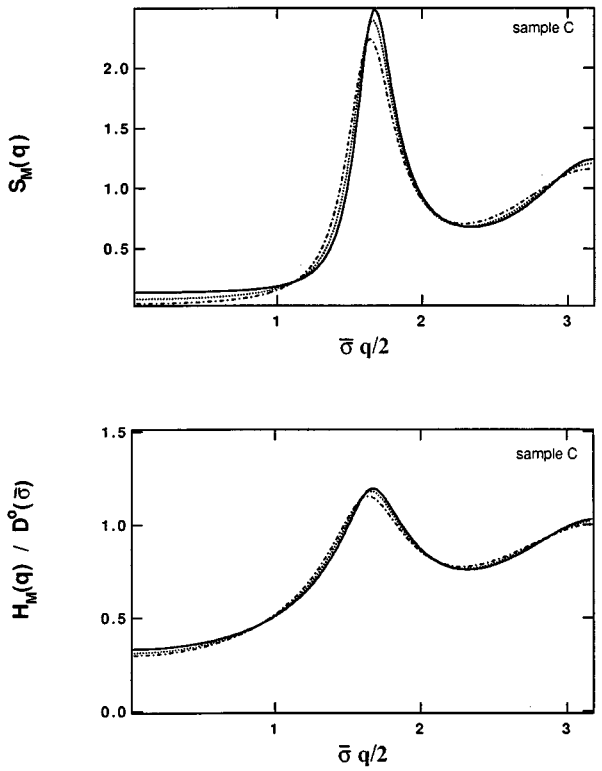

FIG. 6. Test of the sensitivity of the computed $S_M(q)$ (top panel) and $H_M(q)/D^0(\overline{\sigma})$ (bottom panel) to the proposed size dependence of charge polydispersity, represented by Eq. (9), for sample (c) of Table III. The parameters Z^{eff}, ϕ_{fit} are fixed as given in Table III. Full line, $\mu=0$; dotted line, $\mu=1$; dash-dotted line, $\mu=2$.

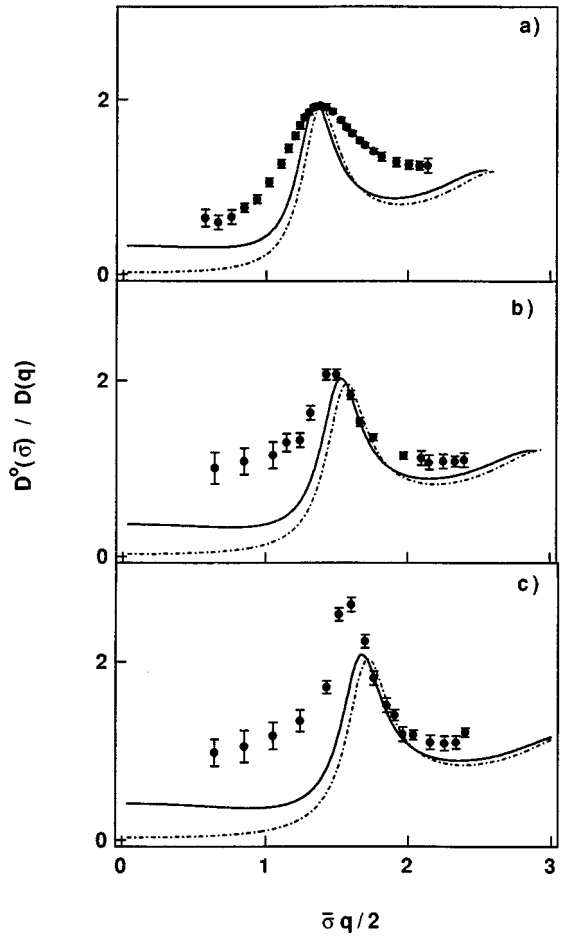

FIG. 7. Inverse of the normalized measurable diffusion coefficient $D_M(q)/D^0(\overline{\sigma})$. Comparison of the DLS measurement (filled circles) with the theoretical results for a size polydispersity $s=0.15$ (full lines) and, for comparison, also for $s=0$ (dashed lines). Parameters for samples (a), (b), and (c) are as summarized in Table III. Here $D^0(\overline{\sigma})=k_BT/(3\pi\eta\overline{\sigma})$, with $\overline{\sigma}=124$ nm.

q value of $S_M(q)$ are affected. The value of $S_M(0)$ decreases as a consequence of larger charge polydispersity and the peak height decreases. This can be attributed to the different contributions of each subcomponent to the scattered light.

D. Short-time dynamics

As discussed in Sec. IV, our model for $D_M(q)$ and $H_M(q)$ are based on the pairwise-additivity approximation of the hydrodynamic mobility tensors, where we have considered terms up to order r^{-11} in the reciprocal interparticle distance. The strong electrostatic repulsion keeps the particles well separated, such that contact configurations are very unlikely. This fact is illustrated in Fig. 5, where $g_{\alpha\alpha}(r)$ is practically zero up to $r=1.6\sigma_\alpha$, where its peak is rather pronounced. Thus the integrals over the far-field mobility tensors converge rapidly. The partial radial distribution functions $g_{\alpha\beta}(r)$ are the only input needed for calculating $H_M(q)$. These functions were obtained in the HNC calculation of $S_M(q)$ while fitting the experimental structure factors. In order to be consistent with static calculations, all particles were assumed to have the same refractive index. The system parameters used in calculating $H_M(q)$ [and $g_{\alpha\beta}(r)$] are summarized in Table III. Once the static properties have been fitted to the experimental results, there are no adjustable parameters in the calculations of the short-time dynamics.

Our experimental and theoretical results for the inverse of the normalized measurable diffusion coefficient $D_M(q)/D^0(\overline{\sigma})$ are displayed in Fig. 7. The quantity used there as normalization $D^0(\overline{\sigma})$ is the Stokes diffusion coefficient evaluated for a mean diameter of 124 nm. The experimental data for $D_M(q)$ are obtained from a first cumulant analysis of the autocorrelation function [cf. Eq. (27)]. Note that $D^0(\sigma)/D_M(q)=S_M(q)[D^0(\overline{\sigma})/H_M(q)]$ reduces to the static structure factor $S(q)$ in the limiting case of a monodisperse system with negligible HIs. The theoretical results for $s=0.15$ and $\mu=0$ are also included in Fig. 7.

The experimental peak height and position are well reproduced in sample (a), but this agreement becomes worse on increasing the volume fraction. Moreover, the width of the principal peak in the experimental $D^0(\overline{\sigma})/D_M(q)$ is consistently underestimated in the calculations. The agreement between theory and experiment may be improved by taking into account many-body HIs at the highest two volume fractions $\phi=0.063$ and 0.048. Previous work on monodisperse systems indicates some improvement of the $H(q)$ obtained from pairwise additivity by calculating the multibody hydrodynamic function $H(q)$ with a $\delta\gamma$ expansion [18–20]. Even without precise quantitative agreement the overall trends are well reproduced by our model, namely, the growth and the shift towards larger values of q of the principal peak, on

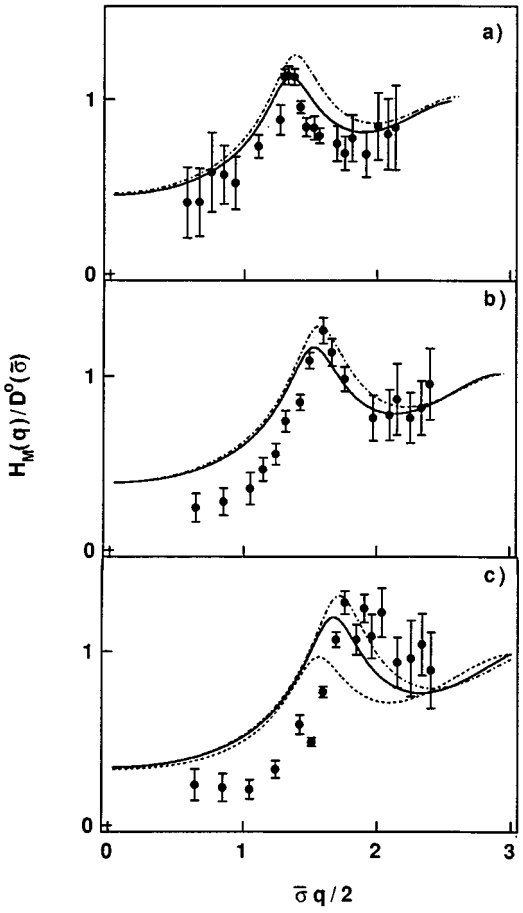

FIG. 8. Measurable hydrodynamic function $H_M(q)$ normalized with $D^0(\overline{\sigma})$ for samples (a), (b), and (c) in Table III. Comparison of the experimental data obtained from DLS and SLS (filled circles) with the theoretical results with constant effective charge ($\mu=0$) for polydispersity $s=0.30$ (dotted line), $s=0.15$ (full line), and $s=0$ (dash-dotted line). Other parameters are as in Table III.

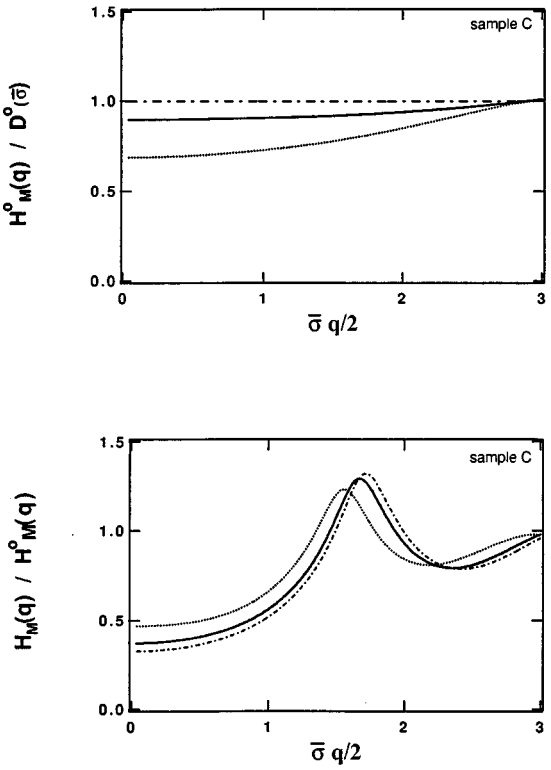

FIG. 9. Hydrodynamic function without hydrodynamic interaction $H^0_M(q)/D^0(\overline{\sigma})$ and calculated measurable hydrodynamic function $H_M(q)/H^0_M(q)$ for sample (c) in Table III. $H^0_M(q)$ denotes the hydrodynamic function in the absence of hydrodynamic interactions. Dotted line, polydispersity $s=0.30$; continuous line, polydispersity $s=0.15$; dash-dotted line, monodisperse case $s=0$. Other parameters are as in Table III.

increasing the volume fraction. This behavior is due to the buildup of interparticle correlations with increasing concentration.

Polydispersity effects can be appreciated by comparing the theoretical results for the monodisperse system with those for $s=0.15$ in Fig. 7. The influence of polydispersity is more pronounced at small wave numbers, where it slows the initial decay of the field auto-correlation functions, producing a substantially smaller $D_M(q)$ relative to the monodisperse suspension. This arises from the fact that the increase of $H_M(q)$ at small q, on enlarging s (Fig. 7), is overcompensated by a larger increase of $S_M(q)$, as one can see from Fig. 3.

We obtain the measurable hydrodynamic function $H_M(q)$ by combining the DLS data of $D_M(q)$ with SLS measurements of $S_M(q)$ according to Eq. (28). We show $H_M(q)$, normalized by $D^0(\overline{\sigma})$, in Fig. 8 together with the corresponding theoretical results for polydisperse ($s=0.15$) and monodisperse ($s=0$) suspensions. The fits of $H(q)$ are better than those for $D^0(\overline{\sigma})/D_M(q)$ due to a fortuitous cancellation of errors. In a manner similar to $S_M(q)$ and $D^0(\overline{\sigma})/D_M(q)$, the principal peak in the experimental $H_M(q)$ becomes more pronounced and moves towards larger values of q for increasing particle concentrations. We further notice that there is a qualitative similarity between the peak position and the oscillatory behavior of $H_M(q)$ and $S_M(q)$. The oscillations of both $H_M(q)$ and $S_M(q)$ become enhanced with increasing ϕ. This enhancement in the case of $H_M(q)$ is particularly manifest at small $q<q_m$, where q_m denotes the peak position of $S_M(q)$. The qualitative behavior of $H_M(q)$ noted above agrees qualitatively with the theoretical results for $s=0.15$. One should keep in mind that there is a certain degree of uncertainty in the experimental data for $H_M(q)$ since it involves the division of two experimentally determined quantities. At low q, the theoretical $H_M(q)$ with polydispersity merges with that for the monodisperse case $H(q)$. The effect of polydispersity becomes visible only for values of q near the main peak, where it reduces $H_M(q)$, relative to the monodisperse case.

To highlight the influence of HIs, it is necessary to consider the ratio $H_M(q)/H^0_M(q)$ instead of $H_M(q)/D^0(\overline{\sigma})$ as shown in our theoretical findings for $H_M(q)/H^0_M(q)$ (with $s=0$, 0.15, and 0.30) in Fig. 9. We have pointed out in Sec. III B that this ratio indicates the importance of HIs and that it is the analog of $H(q)/D^0$ for monodisperse particles. The quantity $H_M(q)/H^0_M(q)$ equals 1 when HIs are negligible, whereas $H_M(q)/D^0(\overline{\sigma})$ is q dependent for $s>0$ even in this limiting case. When HIs are important, $H_M(q)/H^0_M(q)$ becomes explicitly q dependent. The features of $H_M(q)/H^0_M(q)$ that we observe from Fig. 9 are characteris-

tic of charge-stabilized suspensions. We first mention that the effect of HIs is most pronounced at $q \approx 0$, where $H_M(q)/H_M^0(q)$ is substantially smaller than 1. For monodisperse suspensions, this can be attributed to the slowing down of the particle density relaxation induced by the instantaneous HI. Alternatively, we may identify $\lim_{q\to 0} H(q)/D^0$ as the sedimentation coefficient [55,64], at low enough densities for only two-body HIs to be relevant. The sedimentation coefficient is the ratio of the average sedimentation velocity of a colloidal particle in a homogeneous suspension to its value at infinite dilution. Charged particles repel one another when sedimenting, thus reducing the shielding of solvent backflow. This amounts to a strongly reduced sedimentation velocity, i.e., a value $H(0)/D^0$ significantly smaller than 1, particularly compared to suspensions of uncharged particles at the same volume fraction [64]. Very recently, a remarkable nonanalytical volume fraction dependence has been determined for the sedimentation coefficient in experiments with charge-stabilized suspensions of silica spheres, in accordance with theoretical predictions [64]. A similar statistical mechanical identification of the small-q limit of $H_M(q)/H_M^0(q)$ is not possible for polydisperse systems since the scattering amplitudes occur in the defining expressions Eqs. (30) and (32). Considering Fig. 9 we notice further that $H_M(q)/H_M^0(q)$ attains values larger than one around its principal peak and that the peak height increases with increasing ϕ [18]. This behavior is quite typical for charge-stabilized suspensions, where the most important hydro-dynamic contribution to $H_M(q)$ arises from the leading far-field contribution to $\mathbf{B}^{\alpha\beta}(\mathbf{r})$ [18,8]. This contrasts with hard-sphere suspensions, where the maximal value of $H(q)/D^0$ in the monodisperse suspensions never exceeds one and moreover, decreases on increasing ϕ [65]. Hence we can conclude that the effect of HIs is to slow down the initial decay of the field autocorrelation function, at small wave numbers, whereas for charge-stabilized suspensions of low salinity the decay rate is enhanced at $q \approx q_m$. Up to this point all calculations of $H_M(q)$ and $D_M(q)$ were performed for fixed particle charge, i.e., $\mu = 0$.

The additional effect of size-related charge polydispersity on $H_M(q)$ is depicted in Fig. 6(b) for $s = 0.15$ with $\mu = 0$, 1, and 2. The behavior of $H_M(q)/H_M^0(q)$ on varying μ is qualitatively the same as observed for $S_M(q)$ in Fig. 6(a). For the polydispersity used here, there is only a weak dependence of $H_M(q)/H_M^0(q)$ on the amount of charge polydispersity, as quantified by the value of μ. The values assumed by $H_M(q)/H_M^0(q)$ at $q \approx 0$ and $q \approx q_m$ decrease only slightly when μ is enlarged from zero to two.

So far we have considered a polydispersity of $s = 0.15$ to be consistent with our experimental findings. Now, we investigate the importance of size polydispersity in more detail, by varying s from 0 to 0.3 while keeping μ fixed at 0. To calculate $H_M(q)$ for $s = 0.3$, we have used a histogram approximation to the Schulz distribution with $m = 6$ subcomponents; for $s \leqslant 0.15$, three subcomponents are sufficient. Consider first the behavior of the measurable hydrodynamic function without HIs $H_M^0(q)$. According to Eq. (32), $H_M^0(q)$ is simply a form factor weighted superposition of Stokesian diffusion coefficients. Figure 9, top panel, displays our results for $H_M^0(q)/D^0(\overline{\sigma})$, obtained by using the continuous Schulz distribution. This function exhibits a significant q dependence only for large polydispersity (i.e., $s = 0.3$). In principle, one should be able to determine $H_M^0(q) = D_M^0(q)$ from light-scattering experiments performed on sufficiently dilute samples. Here $D_M^0(q)$ denotes the measurable q-dependent diffusion coefficient in the interaction-free case, where $S_M^0(q)$. If it were practical, this would allow for an alternative characterization of the amount of size polydispersity. Unfortunately, the experimental uncertainty due to low photon counting statistics becomes very large for highly diluted, index-matched systems. The fact that $H_M^0(q)$ varies significantly with q for larger s accounts for the differences between $H_M^0(q)/D^0(\overline{\sigma})$ and $H_M(q)/H_M^0(q)$ observable, respectively, from Fig. 9 for the most concentrated sample in our study. As we noted in our discussion of Fig. 8, the effect of size polydispersity on $H_M(q)/D^0(\overline{\sigma})$ is very small for $q \ll q_m$. This feature persists for a polydispersity as large as $s = 0.3$, as shown in Fig. 8, bottom panel; however, due to the variation of $H_M^0(q)$ with s, there is a strong dependence of $H_M(q)/H_M^0(q)$ on s even for small wave numbers. In fact, the overall behavior of $H_M(q)/H_M^0(q)$ as a function of s is similar to that of $S_M(q)$. In both cases, the modulations in q are progressively reduced with increasing polydispersity. Finally, we remark that, contrary to $H_M(q)/H_M^0(q)$, the quantity $H_M^0(q)/D^0(\overline{\sigma})$ becomes smaller than one at large polydispersity (Fig. 8, bottom panel). This illustrates again the fact that $H_M(q)/H_M^0(q)$ is the correct generalization of $H(q)/D^0$ to a polydisperse system and not $H_M^0(q)/D^0(\overline{\sigma})$.

VII. CONCLUDING REMARKS

In this paper we have presented experimental and theoretical results for the equilibrium structure and short-time diffusion in polydisperse suspensions of strongly charged silica spheres, dispersed in a nearly index-matched solvent. We determined the form amplitude averaged static structure factor $S_M(q)$ via static light scattering normalized on the theoretical form factor. We measured diffusion coefficient $D_M(q)$ with dynamic light scattering. Combining SLS data of $S_M(q)$ with DLS data of $D_M(q)$ provided the measurable hydrodynamic function $H_M(q)$. This latter function contains the configuration and form amplitude averaged effects of the HI on the short-time dynamics. With this study, we elucidated the influence of direct electrostatic forces and indirect HIs on the structure and short-time dynamics of charge-stabilized suspensions with a moderate degree of intrinsic size polydispersity. We also tested an existing theoretical description for the hydrodynamic functions of polydisperse charged suspensions [18,8]. This description is based on the pairwise-additivity approximation and far-field expansion of the hydrodynamic mobility tensors, in conjunction with a histogram representative of the Schulz distribution as a model of intrinsic size polydispersity. The partial static correlation functions needed to determine $H_M(q)$ were calculated from the HNC approximation, with system parameters obtained from fitting the HNC structure factor to that determined experimentally. In our calculations, all particles were assumed to have the same refractive index.

Despite the well-known difficulties in measuring $S_M(q)$ and $D_M(q)$ for polydisperse and moderately concentrated suspensions, we believe that our experimental data are in reasonable qualitative agreement with the theoretical predic-

tions. In particular, the experiments confirm the important trends described by the theory. For example, the strong influence of HIs on the short-time dynamics has now been established for polydisperse charge-stabilized suspensions. For small q, HIs tend to slow down the initial temporal decay of the electric field autocorrelation function, whereas the decay rate is enhanced near the position q_m of the principal peak of $S_M(q)$. Thus $H_M(q)H_M^0(q)$ becomes significantly smaller than one for $q \approx 0$ and attains values larger than one around q_m.

There remain some systematic deviations between experiment and theory. In particular, the width of the principal peaks of $H_M(q)$ are systematically larger in the experimental results. The agreement with the theory may be improved by considering multibody hydrodynamic interactions. We have also considered the additional effect of an eventual size dependence of charge polydispersity. Its influence on $H_M(q)$ and $S_M(q)$ was found to be rather weak for the polydispersity of $s=0.15$; however, for larger values of s, our theoretical calculations lead to noticeably different predictions for $S_M(q)$ and $H_M(q)$ when the charge-polydispersity parameter is varied from 0 to 2. Finally, we should emphasize that the size polydispersity of our samples is by no means particularly large; it is smaller than the polydispersity of many other charge-stabilized suspensions. Therefore, a clear implication of this work is the importance of polydispersity for a full quantitive description of these systems.

ACKNOWLEDGMENTS

This work was supported by the National Science Foundation through the Stanford Center for Materials Research and the National Science Foundation Chemistry Division through Grant No. CHE 9520845. We would also like to acknowledge the contributions of A. J. Banchio to this study and Dr. M. A. Tracy for the synthesis of the spheres.

[1] G. K. Batchelor, J. Fluid. Mech. **74**, 1 (1976).
[2] A. B. Glendinning and W. R. Russel, J. Colloid Interface Sci. **89**, 124 (1982).
[3] A. Vrij, J. W. Jansen, J. K. Dhont, C. Pathmamanoharan, M. M. Kops-Werkhoven, and H. M. Fijnaut, Faraday Discuss. Chem. Soc. **76**, 19 (1983).
[4] G. K. Batchelor, J. Fluid. Mech. **131**, 155 (1983).
[5] P. N. Pusey and R. J. A. Tough, Faraday Discuss. Chem. Soc. **76**, 327 (1983).
[6] W. van Megen, R. H. Ottewill, S. M. Owens, and P. N. Pusey, J. Chem. Phys. **82**, 508 (1985).
[7] J. M. Mendez-Alcaraz and R. Klein, Langmuir **8**, 2913 (1992).
[8] G. Nägele, Habilitation thesis, Universität Konstanz, 1994 (unpublished).
[9] R. B. Jones and P. Pusey, Annu. Rev. Phys. Chem. **42**, 137 (1991).
[10] W. Hess and R. Klein, Adv. Phys. **32**, 173 (1983).
[11] P. N. Pusey, J. Phys. A **11**, 119 (1978).
[12] P. N. Pusey, H. M. Fijnant, and A. Vrij, J. Chem. Phys. **77**, 4270 (1982).
[13] J. W. Jansen, C. G. de Kruif, and A. Vrij. J. Colloid Interface Sci. **114**, 481 (1986).
[14] A. van Blaaderen, J. Peetermans, G. Maret, and J. K. G. Dhont, J. Chem. Phys. **96**, 4591 (1992).
[15] B. J. Berne and R. Pecora, *Dynamic Light Scattering* (Wiley, New York, 1976).
[16] P. N. Pusey and R. J. A. Tough, in *Dynamic Light Scattering: Application of Photon Correlation Spectroscopy*, edited by R. Pecora (Plenum, New York, 1985).
[17] D. W. Schaefer and B. J. Berne, Phys. Rev. Lett. **32**, 1110 (1974).
[18] G. Nägele, O. Kellerbauer, R. Krause, and R. Klein, Phys. Rev. E **47**, 2562 (1993).
[19] G. Nägele, B. Steininger, U. Genz, and R. Klein, Phys. Scr. **T55**, 119 (1994).
[20] G. Nägele, B. Mandl-Steininger, and R. Klein, Prog. Colloid Polym. Sci. **98**, 17 (1995).
[21] A. P. Philipse and A. Vrij, J. Chem. Phys. **88**, 6459 (1988).
[22] M. B. Weissman, J. Chem. Phys. **72**, 231 (1980).
[23] P. N. Pusey and W. van Alegen, J. Chem. Phys. **80**, 3513 (1981).
[24] R. Krause, B. D'Aguanno, J. M. Mendez-Alcaraz, G. Nägele, R. Klein, and R. Weber, J. Phys. Condens. Matter **3**, 4459 (1991).
[25] B. D'Aguanno, R. Krause, J. M. Mendez-Alcaraz, and R. Klein, J. Phys. Condens. Matter **4**, 3077 (1992).
[26] B. J. Ackerson, P. N. Pusey, and R. J. Tough, J. Chem. Phys. **76**, 1279 (1982).
[27] R. J. A. Tough, P. N. Pusey, H. N. W. Lekkerkerker, and C. van den Broeck, Mol. Phys. **59**, 595 (1986).
[28] I. M. de Schepper, E. G. D. Cohen, P. N. Pusey, and H. N. W. Lekkerkerker, J. Phys. Condens. Matter **1**, 6503 (1989).
[29] B. D'Aguanno and R. Klein, Phys. Rev. A **46**, 7652 (1992).
[30] S. R. Aragon and R. Pecora, J. Chem. Phys. **64**, 2395 (1976).
[31] S. Alexander, P. M. Chaikin, P. Grant, G. J. Morales, P. Pincus, and D. Hone, J. Chem. Phys. **80**, 5776 (1984).
[32] E. J. W. Verwey and J. T. G. Overbeek, *Theory of the Stability of Lyophobic Colloids* (Elsevier, New York, 1948).
[33] L. Blum and G. Stell, J. Chem. Phys. **71**, 42 (1979).
[34] W. L. Griffith, R. Triolo, and A. L. Compere, Phys. Rev. A **33**, 2197 (1986); **35**, 2200 (1987).
[35] A. Vrij, J. Colloid Interface Sci. **90**, 110 (1982).
[36] G. A. Schumacher and T. G. M. van de Ven, Faraday Discuss. Chem. Soc. **83**, 75 (1987).
[37] P. N. Pusey, in *Liquids, Freezing and Glass Transition: II*, edited by J. P. Hansen, D. Levesque, and J. Zinn-Justin (North-Holland, Amsterdam, 1991).
[38] J. P. Hansen and I. R. McDonald, *Theory of Simple Liquids*, 2nd ed. (Academic, London, 1986).
[39] N. H. March and M. P. Tosi, *Atomic Dynamics in Liquids* (Macmillan, London, 1976).
[40] G. Nägele, P. Baur, and R. Klein, Physica A (to be published).
[41] B. Chichocki, B. U. Felderhof, K. Hinsen, E. Wajnryb, and J. Blawzdziewicz, J. Chem. Phys. **100**, 3780 (1994).
[42] R. B. Jones and G. S. Burfield, Physica A **111**, 562 (1982).
[43] C. W. J. Beenakker and P. Mazur, Phys. Lett. **98A**, 22 (1983).

[44] C. W. J. Beenakker and P. Mazur, Physica A **126**, 349 (1984).
[45] C. W. J. Beenakker and P. Mazur, Physica A **120**, 388 (1983).
[46] U. Genz and R. Klein, Physica A **171**, 26 (1991).
[47] M. A. Tracy and R. Pecora, Macromolecules **25**, 337 (1992).
[48] W. Stöber, A. Fink, and E. Bohn, J. Colloid Interface Sci. **26**, 62 (1968).
[49] G. H. Bogush, M. A. Tracy, and C. F. Zukoski, J. Non-Cryst. Solids **104**, 95 (1988).
[50] A. P. Philipse and A. Vrij, J. Colloid Interface Sci. **128**, 121 (1989).
[51] A. K. van Helden, J. W. Jansen, and A. Vrij, J. Colloid Interface Sci. **81**, 354 (1981).
[52] A. P. Philipse, C. Smits, and A. Vrij, J. Colloid Interface Sci. **129**, 335 (1989).
[53] W. Eimer and R. Pecora, J. Chem. Phys. **94**, 2324 (1991).
[54] G. R. Alms, D. R. Bauer, J. I. Brauman, and R. Pecora, J. Chem. Phys. **58**, 5570 (1973).
[55] W. B. Russel, D. A. Saville, and W. R. Schowalter, *Colloidal Dispersions* (Cambridge University Press, Cambridge, 1989).
[56] S. H. Kim and P. M. Cotts, J. Appl. Polym. Sci. **42**, 217 (1991).
[57] R. J. Lewis, Ph.D. thesis, Stanford University, 1983 (unpublished).
[58] P. N. Pusey and W. van Megen, Physica A **157**, 705 (1989).
[59] T. Okubo, Langmuir **10**, 1695 (1994); private communication.
[60] A. van Blaaderen and A. Vrij, Langmuir **8**, 2921 (1992).
[61] N. J. Wagner, G. G. Fuller, and W. B. Russel, J. Chem. Phys. **89**, 1580 (1988).
[62] B. L. Johnson and J. Smith, in *Light Scattering from Polymer Solutions*, edited by M. B. Huglin (Academic, New York, 1972), Chap. 2.
[63] Y. Rosenfeld and N. W. Ashcroft, Phys. Rev. A **20**, 1208 (1979).
[64] D. M. E. Thies-Weesie, A. P. Philipse, G. Nägele, B. Mandl-Steininger, and R. Klein, J. Colloid Interface Sci. **176**, 43 (1995).
[65] C. W. J. Beenakker, Ph.D. thesis, Rijksuniversiteit Leiden, 1984 (unpublished).